NEW REMOTELY-OPERATED RAMAN-MIE-RAYLEIGH LIDAR IN THE HIGH CANADIAN ARCTIC

Graeme J. Nott, Matthew E. W. Coffin, Line Bourdages, Jonathan G. Doyle, Thomas J. Duck

Department of Physics and Atmospheric Science, Dalhousie University, Halifax NS B3H 3J5 Canada
E-mail:graeme.nott@dal.ca

ABSTRACT

A lidar designed for remote operation in the high Canadian Arctic has been constructed. It operates with seven channels at both green and UV wavelengths and will measure rotational Raman and Rayleigh temperatures, particulate and molecular backscatter, and water vapor content in the lower and middle atmospheres. Presented here is a description of this new Raman-Mie-Rayleigh lidar.

1. INTRODUCTION

The Canadian Network for the Detection of Atmospheric Change (CANDAC), a collaboration between eight Canadian university departments and Environment Canada, is currently installing and operating atmospheric instruments at Eureka, Ellesmere Island, Canada (79°59'N, 85°56'W). Two of CANDAC's major investigative themes revolve around atmospheric energy transfer through both radiative and dynamic processes. As contributors to these themes, Dalhousie University has constructed a Raman-Mie-Rayleigh lidar and installed it at the Zero Altitude PEARL Auxiliary Laboratory (ØPAL) at Eureka. ØPAL has an elevation of only 10m, facilitating measurements from as close to sea level as an instrument allows. Co-located are a millimeter cloud and VHF wind radar, an ozone DIAL and high-spectral resolution lidar, an atmospheric emitted radiance interferometer, a microwave radiometer, and sun and star photometers. This suite of instruments allows a significant number of complementary datasets in the lower and middle atmosphere to be taken at this one site.

The CANDAC Raman Lidar (CRL) is built around two Nd:YAG lasers, one operating at the second harmonic of 532nm, the other at the third, 355nm. The collector is a 1m diameter Dall-Kirkham telescope which is aligned to a 7-channel, free-space polychromator.

In the visible regime, measurements of elastic and vibrational Raman scattering of N_2 will provide backscatter and extinction coefficient profiles. Rotational Raman measurements of N_2 and O_2, when calibrated to local, twice-daily radiosondes, give tropospheric temperature and Rayleigh scattering allows stratospheric temperature calculations. In the UV, elastic, N_2 vibrational Raman, and H_2O vapor vibrational Raman channels allow profiles of extinction and water vapor mixing ratio to be measured.

Eureka is very remote which makes having a dedicated operator on site for long-term data accumulation prohibitively expensive. The system was designed from the beginning to be remotely operable over a low-bandwidth satellite data link. The entire laboratory and lidar; from the roof hatch, to laser operation and alignment, data collection, and safety systems are controlled with custom software.

2. SYSTEM DESCRIPTION

The CRL is housed in a modified shipping container (Container and Trailer Services, Dartmouth NS, Canada). A small office at one end is separated from the laboratory space by an instrument rack and shelving. On a single optical table are the lasers, outgoing optics, and polychromator. At the far end is the telescope which is suspended through a cut-out in the table. In the roof is a borofloat window with a central, laser-quality anti-reflection coated window through which the outgoing beams pass. A 1.5m high box surrounds the window on the roof of the container, this shades the window and provides some protection from the elements and temperature gradient. On top of the box is a motorized hatch.

System specifications are given in table 1.

Table 1: System specifications.

Transmitter	
Visible laser	Continuum Surelite III-10 doubled and seeded
Wavelength	532.08nm
Pulse energy	380mJ
Ultraviolet laser	Continuum Surelite III-10 tripled
Wavelength	354.72nm
Pulse energy	240mJ
Repetition rate	10Hz
Beam expansion	$\times 6$
Outgoing divergence	0.1mrad
Receiver	
Telescope type	Dall-Kirkham
Telescope Diameter	1m
Field of View	0.3–2mrad

2.1. Transmitter

This is a dual wavelength system operating at 532 and 355nm. To ensure high power and good beam quality at both wavelengths, two separate lasers were used, Continuum Surelite III-10's. The lasers produce high energy 4ns

pulses at a repetition rate of 10Hz. They do not require external water cooling and consume only 2.1kW each, important considerations when operating at a remote site. To ensure a stable, narrow linewidth for the rotational Raman temperature measurements, the doubled laser is injection seeded with a temperature-stabilized fiber laser.

Figure 1 shows the layout of the lidar system. The residual 1064 and 532nm beams are dumped (although the system has been set up to be easily extended into the NIR, this facility is not currently being used) and the main beams coaligned with a short wave pass dichroic (transmit 355, reflect 532nm), labelled A in figure 1. Both beams are then expanded with a $\times 6$ spherical beam expander, the angles of which were set to minimize astigmatism in the outgoing beam.

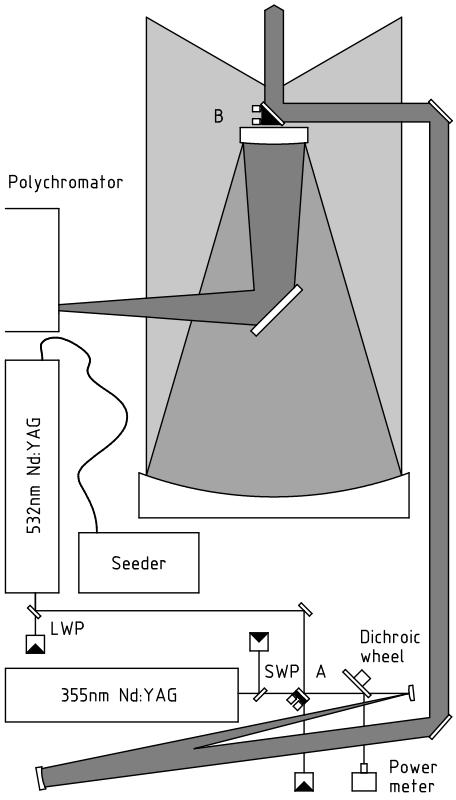

Figure 1: Schematic of the lidar. A long-wave pass dichroic (LWP) removes the residual NIR while a short-wave pass (SWP) removes residual visible and NIR from the UV beam. Dichroic A is a SWP that coaligns the green and UV beams and has stepper motor actuators to align the green beam to the telescope FOV. After expansion, a final 4" mirror, B, is used to steer the UV beam into the telescope FOV. See section 2.1 for details.

The output of each laser can be measured individually with an Ophir power meter. Laser light is reflected onto the thermal head by a computer controlled filter wheel containing a 532nm dichroic, a straight-through position, and a 355nm dichroic. Whenever a power measurement is required, for example when angle tuning the harmonic crystals, both lasers are shuttered, the dichroic wheel rotated from the straight-through position to the appropriate dichroic, and then one of the laser shutters opened. The process is reversed to start collecting atmospheric data. To provide a real-time measure of laser output, two photodiodes detect scattered light off a mirror. Each is behind a wavelength-selective colored glass filter and the outputs are fed into the data accumulation system to be added to the data files.

The system is coaxial. Three 4" turning mirrors are required, the last of which is fitted with computer controlled actuators for beam steering. The two beams are nominally coaligned on the bench and then independently aligned to the telescope's field of view (FOV). The procedure is as follows; the visible laser is shuttered and the UV laser is aligned with the final steering mirror, labelled B in figure 1. The UV laser is then shuttered and the visible laser aligned with the FOV using mirror A. Due to slight beam translation as mirror A is aligned, a second iteration of the alignment procedure is sometimes required.

2.2. Receiver

A custom 1m diameter Dall-Kirkham telescope was made by Optical Structures Inc (Rancho Cordova CA, USA). The telescope was flown to Eureka in a small twin turboprop aircraft and so was designed to be broken down for transit and built up and aligned on site. A tertiary fold mirror, just above table top height, directs collected light into the polychromator.

The polychromator was built by Spectral Applied Research (Richmond Hill ON, Canada). There are seven measurement channels, four in the visible and three in the UV, figure 2 shows the functional layout of the instrument. As with all instruments in this system, the polychromator is completely computer controlled.

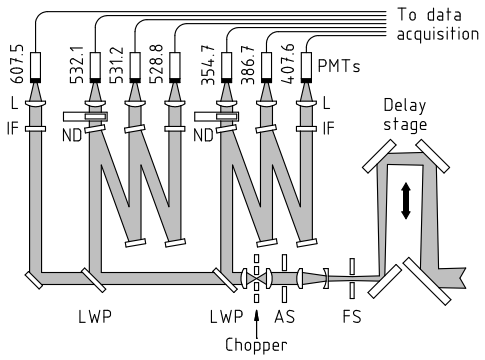

Figure 2: Schematic of the polychromator receiver chain. FS is the field stop, AS the aperture stop. Long wave pass dichroics, LWP, split the light into UV and visible arms and separate the N_2 Raman line from the shorter visible channels. ND are neutral density filter wheels. Each channel has an interference filter, IF, and lens, L, to focus light onto the PMT.

Hamamatsu R7400-03 photomultiplier tubes are used for all channels but the 607nm N_2 Raman line where an extended response R7400-20 PMT is used. Data acquisition is handled by Licel (Berlin, Germany) combined analogue and photon counting transient recorders for the elastic channels and pure photon counting modules for the Raman channels. Sampling rate is 20MHz giving a vertical resolution of 7.5m.

2.2.1. Measurement Optimisation

This system has been designed to take measurements of diamond dust layers very close to ground level through to stratospheric temperatures and detection of polar stratospheric and mesospheric clouds. Several design features were incorporated to optimism the system for measurements in a particular altitude range when required.

- The FOV of the telescope is controlled with a motorized field stop. The range of iris diameters gives FOV's from 0.3–2mrad.
- As scatterers of interest approach ground level the focal plane moves away from the telescope. A motorized optical delay stage moves the field stop relative to the focal plane to accommodate this.
- An second iris controls the effective aperture of the telescope, controlling light levels on all channels. For a given field stop diameter, reducing the aperture of the telescope increases its FOV.
- Light levels on the elastic channels are attenuated when necessary with 5-position neutral density filter wheels.
- A chopper is mounted on a translation stage and can be moved in and out of the beam path. It is used when concentrating on higher altitude measurements and to assist in aligning the outgoing beams to the telescope FOV.

2.2.2. Filter Design

After the chopper a long wave pass dichroic is used to split the UV from the visible light. On the visible side, another long wave pass is used to separate the N_2 Raman line at 607.46nm from those lines closer to the excitation wavelength. The scheme adopted for these wavelengths was developed by Behrendt and Reichardt [1] where a cascade of interference filters transmit one wavelength and reflect the remainder to the subsequent optics in the chain. The visible elastic light is collected first, then the low j-number rotational Raman, and finally the high j-number rotational Raman signal. The UV cascade has a similar sequence with the elastic, then N_2, and finally H_2O channels.

Main considerations when designing the interference filters were the excitation wavelength, the filter's blocking at that wavelength and the bandwidth of the filter that controls the background signal. The rotational Raman channels had additional criteria; the temperature sensitivity, given by position and bandwidth of filters, and temperature uncertainty, which is controlled by the relative center wavelengths of two filters.

Filter specifications for the elastic and vibrational Raman channels were based on existing daytime lidar systems [for example 2; 3; 4]. Unlike for the diatomic channels where, for bandwidths relevant to daytime operation, the temperature dependence is small and diminishing as the bandwidth narrows, the Raman signal from water vapor displays a significant temperature dependence [5]. However, it is still possible to carefully angle-tune the filter so that there is minimal temperature dependence [4; 5].

The lidar is designed to run during day and night time. Given the latitude, where for 33% of the year the sun is continuously below the horizon, two sets of rotational Raman filters were made. A narrow band set for daytime operation and a wide band set for night time. Bandwidths were chosen based on reported manufacturer's specifications in combination with sensitivity and uncertainty calculations described below.

As the atmospheric temperature changes so too does the envelope of the pure rotational Raman lines, an increase in temperature spreads the spectrum, shifting the peak away from the excitation line [see 6, for example]. The judicious choice of two narrow passband filters allows a relative measure of the temperature to be made.

As a starting point for filter design, local radiosonde data was used to obtain relevant temperatures on which to base our calculations. Using a top-hat approximation for the filter passband, the temperature sensitivity, $\partial P_{\mathrm{RR}}/\partial T$ where P_{RR} is the rotational Raman photon count, over the range of wavelengths covered by the anti-Stokes branch was calculated as a function of filter center wavelength and bandwidth [7]. The sensitivity is shown in figure 3

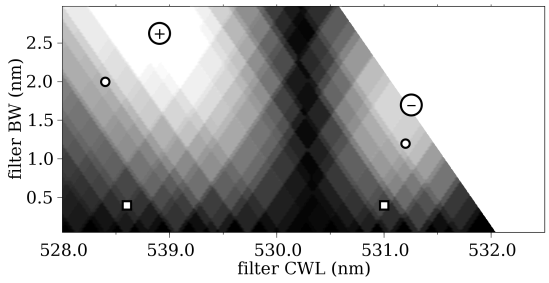

Figure 3: Temperature sensitivity versus filter bandwidth and center wavelength in arbitrary units (white is ± 1, black is 0). Squares are for daytime filters, circles are for the night time filter set.

where for wavelengths shorter than 530.25nm there is a positive dependence with temperature, longer wavelengths have a negative dependence. The empty area contains those combinations of center wavelength and bandwidth that overlap the excitation wavelength.

Assuming Poissonian statistics in the measured signal, the temperature uncertainty was calculated for a given set of filter bandwidths [7] and is shown in figure 4 for both the daytime and night time filters.

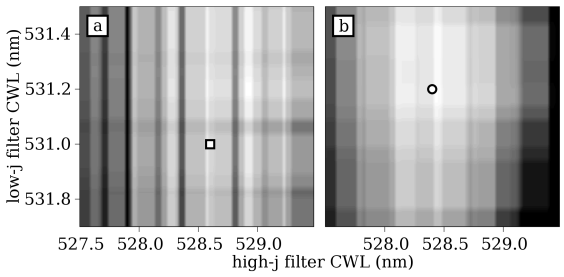

Figure 4: Temperature uncertainty versus filter center wavelength in arbitrary units (white is 0, black is 1) for daytime, (a), and night time, (b), filters.

After an iterative analysis of the various filter characteristics and the trade-off's between the ideal performance and manufacturing tolerances, the optimized interference filter specifications for the system were chosen and are given in table 2.

Table 2: Filter Specifications

Channel	CWL(nm)	BW (nm)	AOI
UV Elastic	354.72	0.35	10°
UV N_2	386.69	0.40	10°
UV H_2O	407.57	0.25	0°
Visible Elastic	532.08	0.35	10°
Visible N_2	607.46	0.40	0°
Rotational Raman			
Low-j (Day)	531.00	0.40	10°
High-j (Day)	528.60	0.40	0°
Low-j (Night)	531.20	1.20	10°
High-j (Night)	528.40	2.00	0°

2.3. Software

This system and laboratory was designed to be remotely operable over the satellite communications link. To facilitate this, while keeping bandwidth requirements to a minimum, custom software was written in Python. An overview of the program structure is shown in figure 5.

The laboratory computer runs a server-side program which controls instrument power through relays and a power controller, and instrument communications through RS232, RS485, and ethernet serial connections. When prompted, the server will turn on the power to the lasers, mirror mount actuators, data acquisition modules, open the roof hatch, etc. Once powered, communications with the relevant instruments is established.

With the client-side GUI, the operator tunes the laser harmonic crystals, aligns the beams to the telescope FOV,

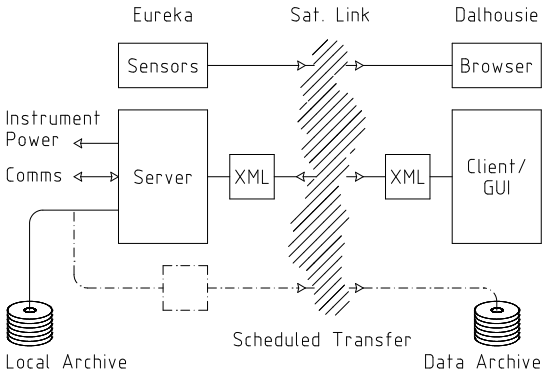

Figure 5: Simplified lidar control software structure. See text for details.

and selects measurement parameters. Data traffic is minimized and passed across the satellite link via XML. Real time data may be passed back to the client in a compressed 'quick-look' form for quality control. The server-side also archives all the data locally and compresses it for a batch transfer with other CANDAC instrument datasets.

For safety and security, the communications link is actively monitored by the server which puts the system into a safe state upon sensing any disconnection. To monitor the laboratory independently of the computer, we installed a stand-alone webserver (AKCP CameraProbe 8) with sensors that measure temperature/humidity, the state of the roof hatch, operation of the air handling system, and the laboratory smoke detector alarm. Security cameras connected to this same webserver are used for visual inspection.

ACKNOWLEDGEMENTS

Construction of the Dalhousie Raman Lidar was supported by the Canadian Foundation for Innovation, the Nova Scotia Research and Innovation Trust, and the National Sciences and Engineering Research Council of Canada.

REFERENCES

[1] Behrendt, A. & Reichardt, J. 2000, Appl. Optics, 39, 1372

[2] Behrendt, A., Nakamura, T., & Tsuda, T. 2004, Appl. Optics, 43, 2930

[3] Goldsmith, J. E. M., Blair, F. H., Bisson, S. E., & Turner, D. D. 1998, Appl. Optics, 37, 4979

[4] Whiteman, D. N., Demoz, B., Di Girolamo, P., et al. 2006, J. Atmos. Oceanic Technol., 23, 157

[5] Whiteman, D. N. 2003, Appl. Optics, 42, 2571

[6] Cooney, J. 1972, J. Appl. Meteorol., 11, 108

[7] Behrendt, A. & Weitkamp, C. 2001, in Advances in laser remote sensing: Selected papers presented at the 20th ILRC, ed. A. Dabas, C. Loth, & J. Pelon, 113–116